JOURNAL OF CATALYSIS 108, 283–293 (1987)

Characterization of MoY Zeolites Prepared by Aqueous Ion Exchange

HUANG MINMING[1] AND RUSSELL F. HOWE[2]

Chemistry Department, University of Auckland, Private Bag, Auckland, New Zealand

Received August 19, 1986

The characterization of MoY zeolites prepared by aqueous ion exchange is described. Zeolites containing up to 5 Mo per unit cell have been obtained. The ion exchange produces a zeolite containing Mo^{+6}, acidic protons, and adsorbed pyridine. Activation by heating *in vacuo* causes loss of pyridine and reduction of up to 18% of the molybdenum to Mo^{+5}. Further reduction cannot be achieved by heating in H_2 up to 700°C. EPR spectra of Mo^{+5} species indicate that molybdenum cations occupy sites both in the supercages and the β cages of the zeolite.

INTRODUCTION

The catalytic importance of molybdenum has prompted numerous attempts to introduce molybdenum cations into zeolites. Gallezot *et al.* first showed that decomposition of $Mo(CO)_6$ adsorbed into zeolite HY produced oxidized molybdenum species through reaction of zerovalent molybdenum with zeolite protons (*1*). Later studies have characterized the MoHY zeolites in more detail (*2, 3*), and catalytic properties have also been reported (*4, 5*). Lunsford *et al.* attempted solid-state ion exchange of HY with $MoCl_5$, but found extensive decomposition of the zeolite lattice; lattice decomposition was minimized by using the ultrastable form of HY (*6, 7*). Solid-state exchange with $MoCl_5$ has been successfully applied also to H-mordenite (*8*).

In a recent patent Moorehead (*9*) has described aqueous ion exchange of molybdenum into NaY using MoO_2Cl_2 in low pH solution. We have undertaken a detailed study of the MoNaY produced by this aqucous ion exchange method with the objectives of characterizing the molybdenum species in the zeolite and comparing them with those in MoHY prepared by decomposition of $Mo(CO)_6$. Such characterization is a necessary prelude to further study of the catalytic properties of molybdenum zeolites, which will be described in subsequent publications.

EXPERIMENTAL

Molybdenum exchanged Y zeolites were prepared according to the patent (*9*) in the following manner: NaY (Strem Chemicals, Lot No. 10779-5) was placed in a beaker containing distilled water and heated while stirring to 65°C. The pH was adjusted sequentially to 4.0 with 1 *M* HCl, to 6.5 with pyridine, then to 3.7 with 1 *M* HCl. Solid MoO_2Cl_2 (prepared from MoO_3 as described in (*10*)) was added slowly to the solution maintained at 55–75°C together with further pyridine to hold the pH at between 3.3 and 4.2. The light yellow slurry formed was then filtered, washed three times with distilled water, and dried in air at 120°C. A reference sample containing no molybdenum (labeled R) was prepared by following the above procedure without adding MoO_2Cl_2.

The Na and Al contents of the NaY zeolite starting material were determined

[1] Permanent address: Department of Modern Chemistry, University of Science and Technology of China, Hefei, Anhui, Peoples Republic of China.

[2] Correspondence to this author.

0021-9517/87 $3.00

by X-ray fluorescence and atomic absorbtion spectrophotometry (AAS). The Mo, Na, and Al contents of the MoY and R samples were then analyzed by AAS, and the Mo contents verified by chemical analysis (the thiocyanate (*11*) method). Surface areas were determined by N_2 adsorption at −196°C (BET method) using a Micromeritics Accusorb instrument, and X-ray powder diffraction measurements employed a Philips PW1130 instrument (Cu$K\alpha$ radiation).

EPR spectra of zeolite samples were measured in a high vacuum cell fitted with a quartz side-arm, using a Varian E4 spectrometer operating at 9.5 GHz. DPPH (g = 2.0036) was used to calibrate g-values, and spin concentrations were estimated by numerical double integration of the first derivative spectra and comparison with the Varian strong pitch standard (calibrated against a single crystal of $CuSO_4$). Computer simulated EPR spectra were obtained on an IBM4341 using the program SIM13 (*12*).

Zeolite samples for infrared experiments were pressed into self-supporting wafers (ca. 5 mg cm^{-2}) at 20 tons and mounted in a conventional high vacuum infrared cell which permitted the zeolite to be heated in a furnace region then moved magnetically into the infrared beam. Spectra were also measured in air (for the purpose of checking the zeolite crystallinity) from 5 mm KBr pellets mounted in a beam condenser. A Nicolet 5DX Fourier transform infrared spectrophotometer operating at 4 cm^{-1} resolution was used, and typically several hundred 1-sec scans of the region 4600–400 cm^{-1} were averaged.

X-ray photoelectron spectra were obtained on a Vacuum Generators ESCALAB spectrometer with Al$K\alpha$ radiation at a resolution of 1.5 eV. Zeolite samples were sprinkled onto double-sided adhesive tape, and a binding energy reference chosen as Si(2p) = 102.8 eV. Peak areas were quantitatively integrated and Si/Al, Mo/Al, and Na/Al ratios calculated from Scofield cross sections assuming the mean free path and transmission function terms to cancel (*21*).

RESULTS

Chemical Composition and Characterization

The results of chemical analysis of three different MoY samples are given in Table 1. The Al, Na, and Mo contents of the zeolites were determined by atomic absorbtion spectrophotometry and the H^+ content by difference (assuming each Mo replaces 2 Na^+ as MoO_2^{+2}). Also shown for comparison are the compositions of the NaY starting material and an NaY sample (R) subjected to the same chemical treatment as the ion exchanged samples without MoO_2Cl_2. Back-exchange of the MoY samples was attempted by heating the zeolite in 10% sodium acetate solution at 70°C for 40 min; the Mo content of the resulting filtrates are expressed in Table 1 as a percentage of the molybdenum originally in the zeolite.

The surface composition of the sample M3 was determined by XPS. The binding energies and molar concentration ratios of

TABLE 1

Chemical Compositions[a]

Sample		Al	Na	Mo	H[b]	% Exchange[c]	% Back exchange[d]
NaY	wt%	11.78	10.03	0		0	—
	n	56	56	—	—		
R	wt%	11.9	7.3	0		28	—
	n	56.5	40.7	—	15.8		
M1	wt%	—	—	0.3		—	ca. 100
	n	—	—	0.4	—		
M2	wt%	10.4	4.0	1.9		60	53
	n	49.4	22.3	2.5	22.1		
M3	wt%	11.3	5.6	3.7		44	63
	n	53.7	31.2	4.9	12.7		

[a] NaY by X-ray fluorescence, all others by atomic absorbtion spectrophotometry.

[b] Calculated assuming all Mo exchanged as MoO^{2+}_2.

[c] Based on Na^+ lost from zeolite.

[d] Fraction of Mo removed by single ion exchange with sodium acetate, as described in text.

[e] Number per unit cell, based on NaY unit cell composition.

[f] The temperatures of ion exchange and amounts of Mo added to the solution (expressed as Mo : Al ratios) were: M1, 60–73°C, 0.08; M2, 55–65°C, 0.29; M3, 74–80°C, 0.24. EDX analysis revealed no detectable Cl.

TABLE 2

XPS Data for MoNaY

	Binding energies[a] (±0.5 eV)			Molar ratios (±0.05)		
	Mo($3d_{5/2}$)	Al($2p$)	Na($2s$)	Si/Al	Mo/Al	Na/Al
As prepared[b]	232.9	74.5	64.4	4.50	0.09	0.63
Activated 400°C	232.7, 231.5[c]	74.7	64.4	4.44	0.19	0.50
NaY[d]	—			3.10	—	1.50
Mo^{+6} in MoO_3 (*13*)	232.5					
Mo^{+6} in MoO_3–SiO_2 (*14*)	233.0					
Mo^{+5} in MoO_3–SiO_2 (*14*)	231.8					

[a] Referenced to Si($2p$) = 102.8 eV.

[b] Sample M3, bulk composition corresponds to Si/Al = 2.53, Mo/Al = 0.093, Na/Al = 0.58.

[c] Two components separated by deconvolution.

[d] Bulk composition corresponds to Si/Al = 2.43, Na/Al = 1.00.

Si, Al, Na, and Mo in the fresh sample and after activation *in vacuo* are given in Table 2. Also given are the corresponding values for the NaY starting material.

Figure 1 shows X-ray powder diffraction patterns of NaY, the R sample, MoY sample M3, and a physical mixture of NaY and MoO_3. The M3 sample (Fig. 1c) showed three additional weak lines at $2\theta < 10°$, which will be commented on later, but the zeolite diffraction pattern is hardly attenuated relative to the MoO_3 : NaY mixture, indicating retention of crystallinity during ion exchange. This was substantiated further by examining infrared spectra in the zeolite framework region. The surface areas of samples M2 and M3 were determined to be 768 and 782 $m^2\ g^{-1}$, respectively, to be compared with a value of 979 $m^2\ g^{-1}$ for the NaY starting material.

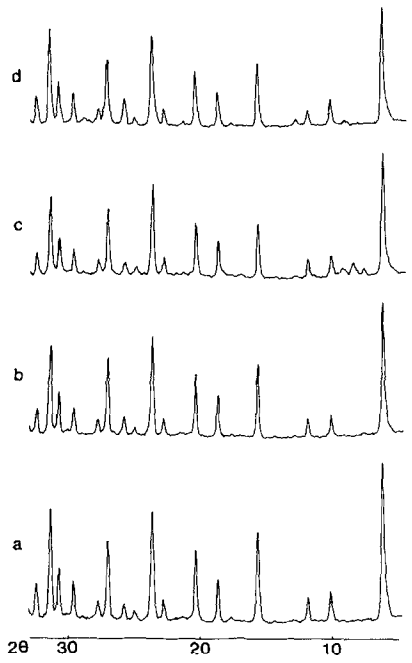

FIG. 1. X-ray diffraction patterns of (a) NaY, (b) R sample, (c) MoNaY sample M3, and (d) physical mixture of MoO_3 and NaY (3.7 wt% Mo).

Activation

The standard activation procedure involved heating the zeolite samples stepwise *in vacuo* to 450°C. Figure 2 shows EPR spectra of sample M3 after activation at 200°C, 300°C, and 450°C. Below 300°C the sample color was unchanged from the light yellow of the fresh zeolite and the EPR spectrum showed only a weak multiplet due to Mn^{+2} impurities (Fig. 2a). At 300°C the color changed to gray and the asymmetric EPR signal shown in Fig. 2b appeared. At higher temperatures the sample color darkened further and the EPR signal grew in inten-

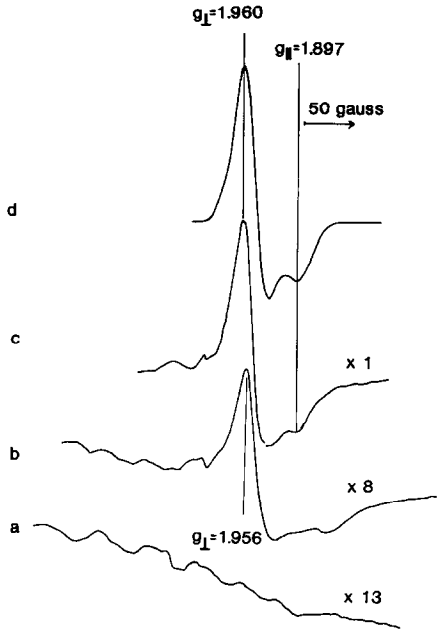

FIG. 2. EPR spectra of MoNaY after activation *in vacuo* at (a) 200°C, (b) 300°C, and (c) 450°C, and (d) computer simulation of the signal in (c) using the g-tensor components shown and linewidths of $\Delta_\perp = 44$ G and $\Delta_\parallel = 50$ G.

sity. A maximum signal intensity was obtained after activation at 450°C for several hours. Further prolonged activation at 450°C caused a decline in the signal intensity, and exposure to H_2 at this temperature caused a further decrease to ca. 1% of the maximum intensity. These changes could be partially reversed by heating in O_2 at 450°C.

The major component of the spectrum in Fig. 2c could be computer simulated with the axial g-tensor components given in Figure 2d. The same signals were formed from the three different MoY samples listed in Table 1, although the time of activation at 450°C necessary to generate the maximum signal intensity varied. For all three samples, the maximum intensities converted to spin concentrations corresponded to about 18% of the total molybdenum content.

Figure 3 shows midinfrared spectra of sample M3 after various stages in the activation sequence. The assignments of the bands are discussed further below. Those due to adsorbed pyridine (around 3000 cm^{-1} and between 1400 and 1650 cm^{-1}) were largely but not completely removed above 300°C and a new band appeared in the ν(OH) region at 3655 cm^{-1} (Fig. 3d). The spectrum in Fig. 3e is that of the R sample containing no molybdenum after activation at 450°C.

Infrared spectra in the framework region (1000–500 cm^{-1}) are shown in Fig. 4. The spectrum of MoY after evacuation at room temperature (Fig. 4a) should be compared with that of NaY (Fig. 4d). The new band at 905 cm^{-1} was not observed in the absence of molybdenum. Evacuation at 200°C removed the 905-cm^{-1} band (Fig. 4b) but it was immediately restored on exposure to air. Activation at 450°C *in vacuo* removed the 905-cm^{-1} band irreversibly (Fig. 4c), but heating to the same temperature in air then cooling to room temperature left the 905-cm^{-1} band unchanged.

Reactivity

Exposure of MoY samples which had been activated at 450°C to ammonia at room temperature caused immediate changes in the EPR spectra. Figure 5a shows, for example, a spectrum obtained by addition of 100 Torr of ammonia to sample M3 at 120°C. This consists of two overlapping axial signals labeled C and D which could be satisfactorily simulated with the g-tensor components shown (Fig. 5b) (the low field features are due to hyperfine splitting from natural abundance ^{95}Mo and ^{97}Mo, which is unusually prominent because of the narrow linewidth of signal C). The relative intensities of C and D were found to depend on the time of exposure to NH_3 and the temperature. By heating in NH_3 to 120°C for an extended period a spectrum could be obtained which consisted exclusively of signal C. Outgassing at 200°C or above removed the new signals and gave spectra such as that shown in Fig. 5c, which contains the original signal of the

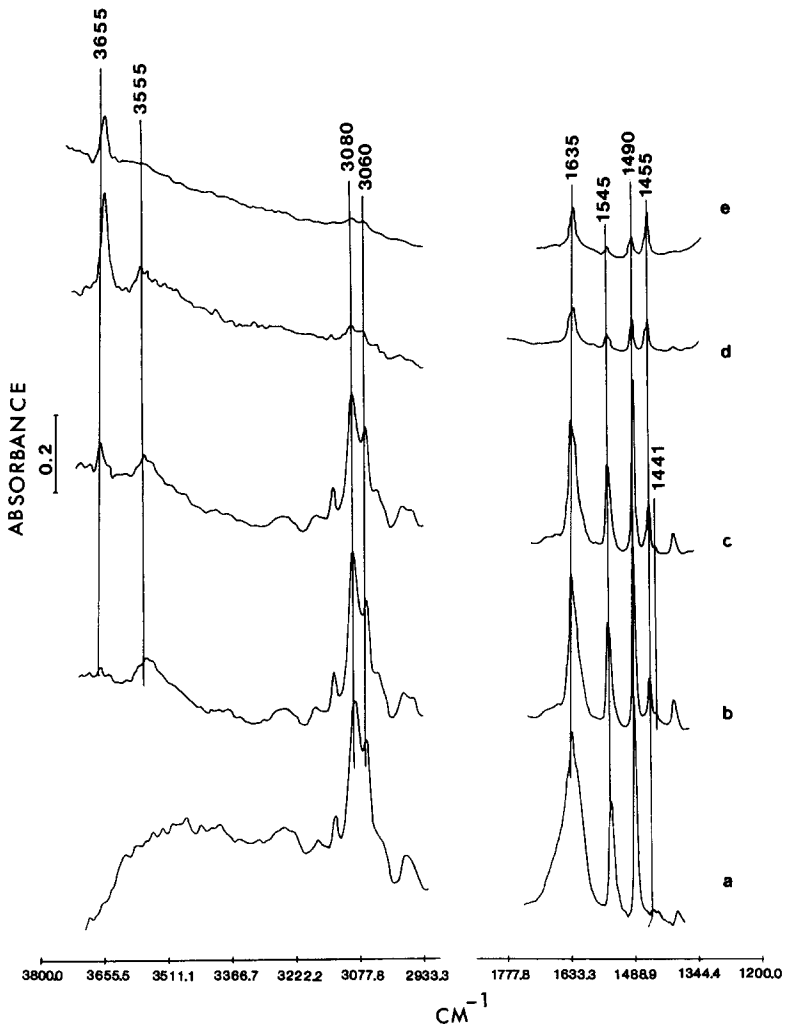

FIG. 3. Infrared spectra of MoNaY after evacuation at (a) room temperature, (b) 200°C, (c) 300°C, and (d) 450°C. (e) R sample after evacuation at 450°C.

activated catalyst (labeled A), plus a second considerably more anisotropic signal labeled B. Figure 5d shows a computer simulation of this spectrum. Further addition of NH_3 restored the signals C and D, although their relative intensities varied through repeated cycles of NH_3 adsorption and outgassing.

The infrared bands of adsorbed NH_3 were superimposed on the residual spectrum of pyridine remaining after activation at 450°C (Fig. 3a). In addition to the formation of NH_4^+ (1450 cm^{-1}) through reaction of NH_3 with the zeolite hydroxyl groups (3655 cm^{-1}), the spectra of adsorbed NH_3 also showed a new band at 1592 cm^{-1} which was removed on outgassing at 200°C (the same temperature required to remove the EPR signals C and D). This band was not formed in an R sample containing no molybdenum.

Exposure of activated MoY samples to pyridine vapor at room temperature caused a small but significant shift in the $g_\perp$ component of the EPR signal A, and a narrowing of the linewidth. Figure 6 shows results of an experiment in which a sample previously treated with NH_3 and then outgassed was exposed to pyridine vapor. The EPR

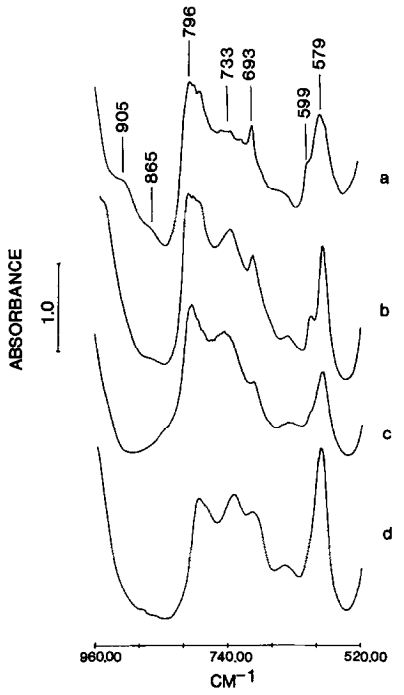

FIG. 4. Infrared spectra of MoNaY after evacuation at (a) room temperature, (b) 200°C, and (c) 450°C. (d) NaY after evacuation at 450°C.

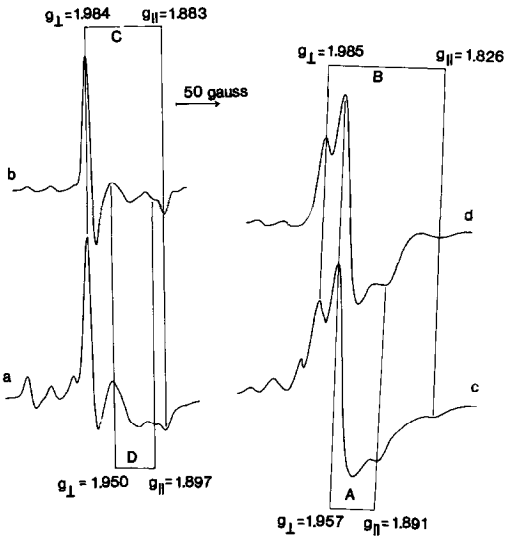

FIG. 5. EPR spectra of MoNaY (a) activated at 450°C and exposed to ammonia at 120°C; (b) computer simulation of (a), using the g-tensor components shown and linewidths of $\Delta_\perp$ = 18 G, $\Delta_\parallel$ = 18 G for signal C, and $\Delta_\perp$ = 38 G, $\Delta_\parallel$ = 38 G for signal D; (c) after subsequent outgassing at 450°C; (d) computer simulation of (c) using the g-tensor components shown and linewidths of $\Delta_\perp$ = 44, $\Delta_\parallel$ = 50 G for signal A, and $\Delta_\perp$ = 28 G, $\Delta_\parallel$ = 58 G for signal B.

signal B formed by NH_3 treatment was unchanged on exposure to pyridine at room temperature, but heating in pyridine to ca. 100°C produced the spectrum in Fig. 6b, which shows the almost complete conversion of signal B into a new much less anisotropic signal E. Also in Fig. 6b is the signal F which results from interaction of pyridine with signal A at room temperature. Outgassing at 300°C or above restored the original signals A and B.

Signals A and B were both affected by exposure to H_2O vapor at room temperature. The effect of H_2O was to decrease the anisotropy of both signals; the g-tensor components of the new signals formed (G and H) are listed in Table 3. Subsequent outgassing at 200°C restored A and B with an approximately twofold reduction in intensity.

Exposure to NO at room temperature caused no changes in the EPR spectra of activated catalysts, and no infrared bands

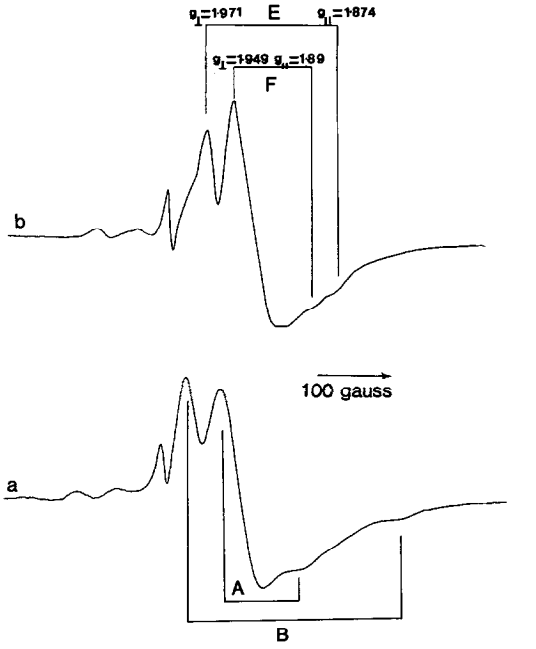

FIG. 6. EPR spectra of MoNaY (a) after adsorption of ammonia and subsequent outgassing at 450°C; (b) exposed to pyridine at 120°C.

TABLE 3

EPR Parameters of Mo^{+5}

	$g_\perp$	$g_\parallel$	$A_\perp/G^a$
MoNaY (this work):			
A (supercage, site II)	1.957	1.897	55
B (β-cage, site II')	1.985	1.826	—[b]
C (B + ammonia)	1.984	1.883	54.3
D (A + ammonia)	1.950	1.897	—[b]
E (B + pyridine)	1.971	1.874	52.5
F (A + pyridine)	1.949	1.89	—[b]
G (B + water)	1.977	1.859	57.5
H (A + water)	1.946	1.878	—[b]
MoHY from $Mo(CO)_6$(3):			
Site II	1.96	1.88	—[b]
Site II'	1.99	1.80	51
Site I or I'	1.96	1.88	51
Ammonia complex	1.982	1.880	56.1
MoHY from $MoCl_5$ (6)	1.956	1.884	—[b]
In MoO_3–SiO_2 (27)	1.947	1.892	45

[a] From natural abundance ^{95}Mo and ^{97}Mo, ±1 G.
[b] Not measured.

due to chemisorbed nitric oxide could be detected.

DISCUSSION

Molybdenum Ion Exchange

The original patent describing the preparation of MoY zeolites from MoO_2Cl_2 suggests that molybdenum is exchanged into the zeolite as the divalent cation MoO_2^{2+} (9). Complete replacement of all Na^+ in the starting NaY would then produce a zeolite containing 28 Mo per unit cell. The highest molybdenum loading achieved in our experiments (sample M3, Table 1) corresponds to ca. 18% of the maximum possible value, which is not inconsistent with the range of 10–50% quoted in the patent. The loss of sodium from the zeolite in the R sample can only be due to replacement by H^+; a significantly larger sodium loss was found for samples containing molybdenum, indicating that ion exchange of molybdenum had occurred to at least some extent. The alternative possibility, that deposition of a molybdenum-containing species occurred on the external surface, is not consistent with the XPS results in Table 2 which show that the surface Mo : Al molar ratio is in good agreement with the value calculated from the overall chemical composition. The ca. 200 $m^2\ g^{-1}$ loss in surface area also implies occupation of the zeolite supercages by molybdenum species, since the X-ray diffraction patterns and low frequency infrared spectra showed no evidence for loss of crystallinity.

Moorehead further reports that the molybdenum ion exchange is almost completely reversible. In our hands this was so only for samples containing low concentrations of molybdenum (e.g., M1), but more than 50% of the molybdenum in higher loading samples was readily removed by a single back-exchange treatment, indicating again that ion exchange is at least a major route by which molybdenum enters the zeolite.

Further indications of the nature of the ion-exchanging species can be gained from the present experiments. The EPR and XPS measurements both suggest Mo^{+6} as the initial valence state of molybdenum. The Mo($3d_{5/2}$) binding energy of 232.9 eV of sample M3 as prepared should be compared with typical values of 232.5 eV for MoO_3 (*13*) and 233.0 eV for Mo^{+6} on molybdena–silica catalysts (*14*), and the absence of an Mo^{+5} EPR signal from freshly prepared samples indicates that no reduction of molybdenum occurs during ion exchange.

The new infrared band appearing at 905 cm^{-1} in freshly prepared catalysts (Fig. 4a) falls in the region characteristic of ν(Mo–O) vibrations. The monomeric MoO_2Cl_2 in the vapor phase has terminal ν(Mo=O) frequencies of 990 cm^{-1} (asymmetric) and 972 cm^{-1} (symmetric) (*15*), while in the solid, which is polymeric, oxide ions bridge adjacent molybdenums and the vibrational frequencies are 909, 867, and 810 cm^{-1} (*16*). The exact nature of the oxomolybdenum species in the zeolite which gives the 905-cm^{-1} band in Fig. 4 cannot be determined from a single vibrational frequency. The frequency is closer to that of an Mo–O

single bond than a terminal Mo=O as in MoO_2Cl_2. Any terminal ν(Mo=O) bands present would however be totally obscured by intense zeolite absorbtion above 950 cm^{-1}. We note also that the 905-cm^{-1} band is sensitive to the coordination state of the molybdenum; it is observed only in the presence of adsorbed H_2O (exposure to air) and in catalysts which have not been activated at high temperatures. The changes in coordination accompanying dehydration may be represented, for example, by the reaction

$$MoO_2(H_2O)_2^{2+} \rightarrow MoO_2^{2+} + 2H_2O$$

where the 905-cm^{-1} band is attributed to the hydrated cation.

The infrared spectra in Fig. 3 show that a large amount of pyridine enters the zeolite during the ion exchange procedure. The vibrational frequencies of pyridine adsorbed in zeolites have been widely studied (*17*). The zeolite as prepared contains the pyridinium cation $C_5H_5NH^+$ (1490, 1545, 1635 cm^{-1}) plus some physically adsorbed pyridine (1490, ca. 1660 cm^{-1}) which is lost on outgassing at 200°C (Fig. 3b). The new band appearing at 1455 cm^{-1} in Fig. 3b on outgassing is due to pyridine coordinated to Al^{+3} (Lewis acid site) (*17*). This band was also formed in the R sample (Fig. 3e). Lewis acidity in faujasite zeolites is associated with the presence of extraframework Al^{+3} cations (*18*). The formation of extraframework Al^{+3} during ion exchange must be due to partial dealumination of the zeolite lattice under the low pH conditions of ion exchange. The XPS data in Table 2 showing Al depletion of the surface layers of the zeolite support this conclusion. It should be emphasized however that the number of Al^{+3} Lewis acid sites is small; never more than ca. 15% of the number of Brønsted sites on which the pyridinium cation is formed.

Since the starting material MoO_2Cl_2 can readily form complexes of the type $MoO_2Cl_2L_2$ with many organic ligands (*19*), the ion exchanging cation may contain coordinated pyridine ligands. There are however no bands in the infrared spectra which can be clearly assigned to pyridine coordinated to molybdenum. The weak band at 1441 cm^{-1} in Fig. 3a–c has been attributed to pyridine coordinated to Na^+, although it has also been pointed out that the vibrational frequencies of coordinated pyridine are not particularly sensitive to the nature of the cation (*20*). The possibility of a contribution to the 1441-cm^{-1} band from pyridine coordinated to molybdenum thus cannot be ruled out. Indirect evidence for the importance of pyridine in the ion exchange comes from experiments in which the same ion exchange procedure was attempted with zeolites mordenite and ZSM-5 (*22*). For the smaller pore zeolites no ion exchange was achieved in the presence of pyridine; X-ray diffraction and XPS showed that molybdenum was deposited on the external surfaces of the zeolites. Ion exchange into mordenite and ZSM-5 could be achieved only in the absence of pyridine, when presumably uncomplexed cations could enter the zeolite pores. In the case of NaY pyridine is necessary to maintain the pH at a high enough level to prevent decomposition of the zeolite, and although the X-ray diffraction patterns showed occasional traces of additional lines due to molybdenum deposited on the external surface (e.g., at about $2\theta = 9°$ in Fig. 1c), such surface deposition occurred to only a minor extent.

Activation

Given that the ion exchange procedure produces a zeolite containing oxomolybdenum cations in the +6 valence state plus adsorbed pyridine, we must then consider the changes occurring during activation to drive off water and pyridine. The EPR spectra in Fig. 2 show clearly that activation *in vacuo* at 300°C or above causes reduction of Mo^{+6} to Mo^{+5}. This is supported by the XPS measurements, which showed the growth of a lower binding energy doublet due to Mo^{+5} on activation.

The EPR signal A formed on activation at 450°C (Fig. 2c) has g-tensor components closely similar to those of Mo^{+5} in MoHY zeolites prepared by adsorption and decomposition of $Mo(CO)_6$ (Table 3). This species thus does not contain coordinated pyridine. Evidence supporting its location in the zeolite supercages is discussed below.

The onset of reduction of Mo^{+6} to Mo^{+5} during activation at 300°C or above correlates with the loss of infrared bands due to adsorbed pyridine, particularly between 300 and 450°C. The pyridinium cation decomposes more readily than pyridine coordinated to Lewis acid sites, and the loss of $C_5H_5NH^+$ is accompanied by the appearance of a ν(OH) band at 3655 cm^{-1}. This band is assigned to hydroxyl groups located in the supercages of HY (*23*). The overall reduction of Mo^{+6} during activation can thus be represented by

$$Mo^{+6} + PyH^+ \rightarrow 2H^+ + Mo^{+5} + \text{pyridine decomposition products}$$

although the actual reducing species may be pyridine decomposition products rather than PyH^+. The extent of reduction (never more than 18% of the total Mo^{+6} content) may be determined by the amount of pyridine present, although it is clear also that molybdenum in NaY is unusually resistant to reduction, since the Mo^{+5} concentration could not be enhanced by heating in H_2 to 700°C.

The changes in the low frequency infrared spectra upon activation (Fig. 4) are consistent with the above description. The irreversible loss of the 905-cm^{-1} ν(Mo–O) band on activation above 200°C implies reduction and/or change in the coordination state of molybdenum. The zeolite band at 579 cm^{-1} due to vibration of the double six-ring (D6R) in the faujasite structure (*24*) sharpens on initial activation due to loss of water (a similar change occurred in the R sample containing no molybdenum), then broadens again at higher temperature. Such broadening was not observed in the R sample. Perturbation of the D6R vibration accompanying dehydration of CaY has been attributed to migration of Ca^{+2} cations into site I within the D6R (*25*). The broadening observed for MoNaY is thus attributed to migration of molybdenum cations into sites in or adjacent to the D6R (sites I or I′). The zeolite structure-sensitive band at 796 cm^{-1} is not affected by activation, confirming that there is no loss of structure. The additional weak bands present at 865 and 599 cm^{-1} in the zeolite as prepared (Fig. 4a) were also found in the R sample and have no counterparts in the spectrum of NaY (Fig. 4d); these may result from the dealumination occurring during ion exchange, since ultrastable zeolites derived from NaY are reported to show additional framework bands (*26*).

Reactivity of MoNaY

The Mo^{+5} species responsible for the EPR signal A interacts immediately with ammonia, pyridine, and water on exposure at room temperature. This species must therefore be located in the supercages of the zeolite. The form of the g-tensor components ($g_\parallel < g_\perp < 2$) is consistent with both distorted tetrahedral and distorted octahedral coordination, but the relatively small anisotropy ($g_\perp - g_\parallel \approx 0.06$) suggests (by comparison with molybdena–silica catalysts, $g_\perp = 1.95$ and $g_\parallel = 1.89$ (*27*)) that species A is a molybdenyl species in distorted octahedral coordination. The g-tensor components of species A are identical to those of a signal (signal D in Ref. (*3*)) formed during decomposition of $Mo(CO)_6$ in HY and attributed to Mo^{+5} in the supercages. Furthermore, the parameters of the new signal C formed by adsorption of ammonia in MoNaY are also closely similar to those of the signal attributed to an Mo^{+5}: ammonia complex in HY (*3*). Our interpretation of the spectrum shown in Fig. 5a is then that the signal D is due to traces of the uncomplexed species A interacting weakly with (solvated by) ammonia in the supercage, whereas signal C is due to a specific

coordination complex of ammonia. The reaction of species A with ammonia can be envisaged to occur via the weakly interacting (solvated) species

$$\underset{(A)}{Mo^{+5}} + NH_3 \rightarrow \underset{(D)}{Mo^{+5}(NH_3)} \rightarrow \underset{(C)}{(Mo \leftarrow NH_3)^{+5}}$$

where the number of coordinated ammonia ligands is unknown, and the Mo^{+5} species may be MoO^{+3} or MoO_2^+. The reaction can be driven to completion by mild heating. Since the β-cages can adsorb up to 2 ammonia molecules per cage (*28*), the ammonia complex responsible for signal C may be located in the β-cages. The suggestion that ammonia adsorption can cause migration of Mo^{+5} into the β-cages is supported by the appearance of a second Mo^{+5} signal (B) not previously present on subsequent outgassing. Signal B is not affected by exposure to pyridine at room temperature and we attribute it to a Mo^{+5} located in the β-cages, probably in site II′ adjacent to the supercages since it does interact with pyridine in the supercages on heating. An Mo^{+5} signal with g-tensor components similar to those of signal B has been attributed to Mo^{+5} in site II′ in MoHY prepared from $Mo(CO)_6$ (*3*).

The first formation of signal B during desorption of ammonia could alternatively be attributed to reduction of Mo^{+6} already located in the β-cages by ammonia. The reversibility of subsequent complex formation with ammonia implies however a degree of mobility of Mo^{+5} cations between β-cage and supercage. In the case of pyridine complex formation can occur only in the supercages and heating is necessary to drive Mo^{+5} cations through the 6 rings from site II′. No new infrared bands of pyridine coordinated to Mo^{+5} could be distinguished from those of other adsorbed pyridine species, but the band appearing at 1592 cm^{-1} on adsorption of ammonia can be attributed to the doubly degenerate bending mode of coordinated NH_3; this vibration occurs at 1613 cm^{-1} for example in ammonia adsorbed on MoO_3 surfaces (*29*).

In the case of water adsorption, both Mo^{+5} species interact with H_2O at room temperature to form two different complexes. Since water can enter both supercages and β-cages, the two complexes formed with adsorbed water are presumed to be located both in the supercages (signal H formed from signal A) and β-cages (signal G formed from signal B), respectively.

The absence of any measurable interaction with nitric oxide was unexpected. Chemisorption of nitric oxide has been widely used as a means of poisoning and titrating active sites on supported molybdena catalysts (*30–34*). A dinitrosyl species containing two coordinated NO ligands has been observed by infrared spectroscopy on alumina- (*31*) and silica-supported molybdena (*32*) catalysts, and in MoHY prepared from $Mo(CO)_6$ (*33*). The site on which the dinitrosyl species is formed has been variously identified as Mo^{+3} (*31*), Mo^{+4} (*32*), and most recently Mo^{+2} (*34*). A paramagnetic molybdenum–nitrosyl adduct has also been detected by EPR spectroscopy in both oxide- and zeolite-supported catalysts derived from $Mo(CO)_6$ (*32, 33*), which is associated with low valent molybdenum. The complete absence of both the infrared active dinitrosyl species and the paramagnetic adduct from ion exchanged MoNaY must mean that the valence states of molybdenum which interact with nitric oxide are not present in the ion exchanged catalyst. The comparison with MoHY prepared from $Mo(CO)_6$ is particularly striking, since these zeolites show otherwise many similarities. We conclude that the ion exchanged zeolites, when pretreated under the conditions used here, do not contain any molybdenum in valence states below +4. This conclusion is consistent with the EPR and XPS observations that the Mo^{+6} initially ion exchanged into the zeolite is much more difficult to reduce than in oxide-supported molybdena catalysts. The Mo^{+5} in the supercages (signal A) can be reduced by heating in H_2, but evidently not below Mo^{+4}.

Conclusions

The experiments described here have shown that the solution ion-exchange procedure produces MoNaY zeolites in which the molybdenum is largely ion exchanged as Mo^{+6}, probably in the form of the dioxocation MoO_2^{+2}. Molybdenum exchange is accompanied by proton exchange but without significant loss of crystallinity. The zeolite as prepared also contains adsorbed pyridine. Subsequent activation causes desorption of water and pyridine, and reduction of some molybdenum to the +5 state. Molybdenum cations are located in both the supercages and in more hidden sites in the zeolite lattice; EPR experiments have provided some information about the location and reactivity of that fraction of the molybdenum which is paramagnetic.

From a catalytic viewpoint, the MoNaY zeolites prepared by aqueous ion exchange differ from the MoHY zeolites prepared from $Mo(CO)_6$ in that they contain no lower valence states of molybdenum. The ion-exchanged zeolites also differ from conventional supported molybdena catalysts in that they contain high concentrations of Brønsted acid sites (ion-exchanged protons). The catalytic consequences of these differences will be reported subsequently.

ACKNOWLEDGMENTS

We acknowledge support of this work by the Donors of the Petroleum Research Fund, administered by the American Chemical Society. The assistance of Mr. A. E. Hughes of C.S.I.R.O. Division of Materials Science, Australia, in obtaining XPS spectra is also acknowledged.

REFERENCES

1. Coudurier, G., Gallezot, M. P., Praliaud, H., Primet, M., and Imelik, B., *C. R. Hebd. Seances Acad. Sci., Ser. C.* **282,** 311 (1976).
2. Gallezot, P., Coudurier, G., Primet, M., and Imelik, B., *ACS Symp. Ser.* **40,** 144 (1977).
3. Abdo, S., and Howe, R. F., *J. Phys. Chem.* **87,** 1713 (1983).
4. Vrinat, M. L., Gachet, C. G., and de Mourgues, L., "Catalysis by Zeolites," p. 219. Elsevier, Amsterdam, 1980.
5. Namba, S., Komatsu, T., and Yashima, T., *Chem. Lett.*, 115 (1982).
6. Dai, P. E., and Lunsford, J. H., *J. Catal.* **64,** 173 (1980).
7. Ward, M. B., and Lunsford, J. H., "Proceedings of 6th International Zeolite Conference, 1983" (D. H. Olson and A. Bisio, Eds.). Butterworths, London, 1984.
8. Johns, J. R., and Howe, R. F., *Zeolites* **5,** 251 (1985).
9. Moorehead, E. L., U.S. Patent 4,297,243 (1981).
10. Zado, F., *J. Inorg. Nucl. Chem.* **25,** 1115 (1963).
11. Vogel, A. I., *et al.*, "Quantitative Inorganic Analysis." Longmans, London, 1966.
12. Lozos, G., Hoffman, B., and Franz, B., "Quantum Chemistry Program Exchange," No. 265, 1974.
13. Swartz, W. E., Jr., and Hercules, D. M., *Anal. Chem.* **43,** 1774 (1971).
14. Ward, M. B., Lin, M. J., and Lunsford, J. H., *J. Catal.* **50,** 306 (1977).
15. Iorns, T. V., and Stafford, F. E., *J. Amer. Chem. Soc.* **88,** 4819 (1966).
16. Adams, D. M., and Churchill, R. G., *J. Chem. Soc. A*, 2310 (1968).
17. Ward, J. W., *in* "Zeolite Chemistry and Catalysis" (J. A. Rabo, Ed.), Vol. 171, p. 118. ACS Monogr., 1976.
18. Jacobs, P. A., and Beyer, H. K., *J. Phys. Chem.* **83,** 1174 (1979).
19. Barlar, J. C., "Comprehensive Inorganic Chemistry," Vol. 3. Pergamon, Elmsford, New York, 1973.
20. Gill, N. S., *J. Inorg. Nucl. Chem.* **18,** 79 (1961).
21. Sexton, B. A., Smith, T. D., and Sanders, J. V., *J. Electron Spec. Rel. Phen.* **35,** 27 (1985).
22. Huang, M., and Howe, R. F., to be published.
23. Eberly, P. E., Jr., *J. Phys. Chem.* **71,** 1717 (1967).
24. Flanigen, E. M., *in* "Zeolite Chemistry and Catalysis" (J. A. Rabo, Ed.), Vol. 171, p. 80. ACS Monogr., 1976.
25. Flanigen, E. M., Khatami, H., and Szymanski, H. A., *Adv. Chem. Ser.* **101,** 201 (1971).
26. Scherzer, J., and Bass, J. L., *J. Catal.* **28,** 101 (1973).
27. Seyedmonir, S., and Howe, R. F., *J. Catal.*, in press.
28. Barrer, R. M., and Gibbons, R. M., *Trans. Faraday Soc.* **59,** 2569 (1963).
29. Groff, R. P., *J. Catal.* **86,** 215 (1984).
30. Howe, R. F., and Kemball, C., *J. Chem. Soc., Faraday Trans. 1* **70,** 1153 (1974).
31. Hall, W. K., and Millman, W. S., *J. Phys. Chem.* **83,** 427 (1979).
32. Kazusaka, A., and Howe, R. F., *J. Catal.* **63,** 447 (1980).
33. Ravines, P., and Howe, R. F., to be published.
34. Hall, W. K., *et al.*, *J. Catal.* **90,** 368 (1984).